Design of a Propeller with Global Minimum Torque

Caleb Robb*
Oklahoma State University, Stillwater, OK, 74078

Matthew N. Gray†
NASA Langley Research Center, Hampton, VA, 23681

Todd A. Ferrante‡
Analytical Mechanics Associates, Hampton, VA 23666

Albion H. Bowers§
NASA Armstrong Flight Research Center, Edwards, CA 93523

Academia, industry, and Government are actively working towards a future where dozens of small to large Unmanned Aerial Systems (UAS) are present within urban environments. In this environment, high noise pollution and inefficiencies have the potential to render these new technologies impractical due to public annoyance and nonacceptance. This study aims to design and analyze a novel propeller design for minimum global torque using an optimization algorithm to find the full three dimensional solution of maximum efficiency. This resulted in a C_l distribution defining the global minimum torque solution for propeller design which corresponded with moving as much lift inboard as possible and reducing lift rapidly at the blade tip. The novel propeller (dubbed *"Prandtl"* propeller) was then compared with the current gold standard in propeller design, a minimum induced loss (MIL) propeller, which had all the same geometric properties *except* for blade twist and produced the same amount of thrust at the same advance ratio. The results of multiple iterations of Prandtl propellers showed an increase in efficiency of *2.0-3.3*% for the Prandtl blade when compared to the equivalent MIL blade. A potential added benefit of this blade design is lower noise generation due to the lower lift loading at the tip reducing the large shear layer intensity which is the point source of noise in propellers. Two major breakthroughs for enabling widespread use of UAS in urban environments are noise reduction and vehicle efficiency, and this new propeller design has the potential to provide both.

I. Nomenclature

α	=	Angle of attack
α_i	=	Induced angle of attack
β	=	Blade Twist
c	=	Local chord value
C_d, C_l	=	2-D drag and lift coefficients
d	=	Overall diameter
dF	=	Incremental value of F
ϕ	=	Blade Inflow Angle
ρ	=	Fluid density
r	=	Local section radius
R	=	Overall radius
Re	=	Reynolds Number
μ	=	Viscosity

*Graduate Research Assistant, Oklahoma State Department of Mechanical and Aerospace Engineering, Student AIAA Member
†Electronics Engineer, NASA Langley Research Center, Aeronautic Systems Engineering Branch, AIAA Member, 4 Langley Blvd., M/S 238
‡Mechanical Engineer, Analytical Mechanics Associates, 21 Enterprise Pkwy, Hampton, VA 23666
§Chief Scientist, NASA Armstrong Flight Research Center, Office of Chief Scientist

V_0 = Free-stream Velocity
V_r = Resultant velocity
ω = Rotational rate

II. Introduction

THE Prandtl Bell Spanload has been a case study in the field of aerodynamics since it was suggested by Prandtl in 1933 as the minimum induced drag condition for a wing with a bending moment constraint. This spanload distribution reallocates the loading to be concentrated more near the root than an elliptical distribution before steeply decreasing to keep the bending moment constant as shown in Fig. 1. This design allows a couple of benefits to present, with the first being an interesting effect on the rolling dynamics of the aircraft [1–3] and the second being a reduction in the induced drag when compared to an elliptically loaded wing with the same root bending moment. With a properly designed wing, this spanloading can present with testable benefits [4] that could increase efficiency over a specific flight envelope.

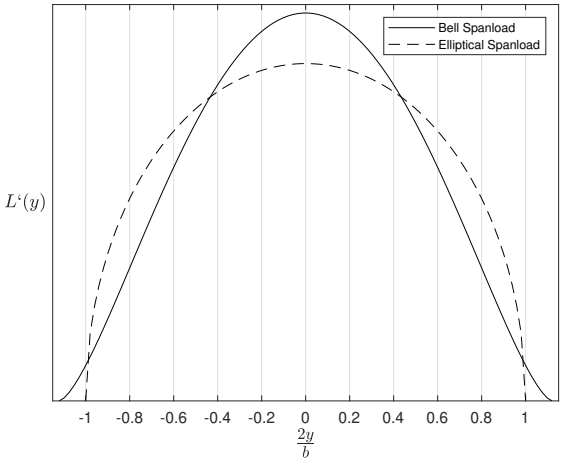

Fig. 1 Wing Loading Distribution Comparison of Bell and Elliptical Spanloads

With promising results showing increased efficiency over specific portions of the flight envelope, an interesting question arises: what if a similar design process was applied to a propeller? The loading on the propeller can be pushed inboard, decreasing the loading on the tip. The idea for implementing this on a propeller started out as a thought experiment: what happens when you treat propellers as a black box and only consider the input (power) and output (thrust)? If rotations per minute (RPM) is held as an independent variable, then power is linearly correlated with torque, so optimizing for global minimum torque will optimize for the most efficient possible propeller design. An optimization algorithm was then made by Bowers et al. in order to find the coefficient of lift (C_l) distribution along a propeller which produces the *global* minimum torque solution (i.e. the minimum total torque across the blade span) [4]. This is the full three dimensional solution for a minimum torque propeller blade, and the basis behind the design and analysis results in this paper.

The algorithm used by Bowers' team optimized the propeller twist by minimizing the overall torque under a constant thrust condition. Calculus of variations was used to find the function of C_l vs r that produced the lowest *total* torque and thus power. A couple assumptions were made in this first attempt at optimizing efficiency in order to simplify the problem initially: (1) the airfoil remains the same across r, (2) the chord remains the same across r (i.e. rectangular chord), and (3) RPM and free-stream velocity (i.e. advance ratio) is held constant in the blade theory analysis of each C_l distribution condition evaluated by the optimizer. The optimizer then found the C_l distribution with the global three dimensional minimum torque solution of a propeller which is shown in Fig. 2 below.

Coincidentally, the optimization algorithm found that the global minimum torque solution is not a minimum induced loss (MIL) propeller - considered the current optimal solution in propeller design [5], [6] - it is a propeller that is loaded more inboard and unloaded at the tip, similar to the Prandtl Bell Spanload. An additional benefit, alongside the

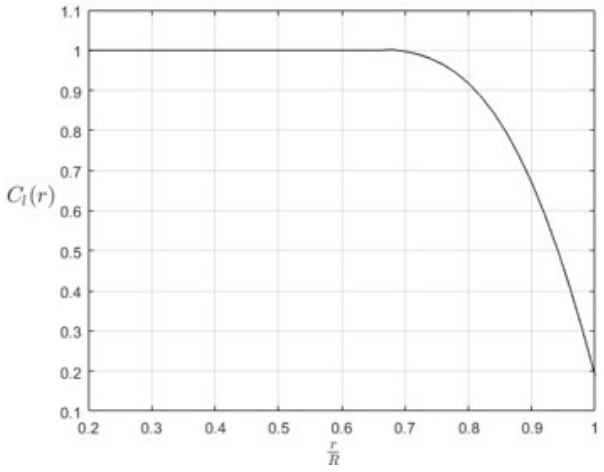

Fig. 2 Coefficient of Lift Distribution Percentage for Global Minimum Torque

efficiency increase predicted, is a possible acoustic effect of unloading the tips since the tip loading has been shown to have a large influence on that acoustic signature [7].

A formal study was never conducted by Bowers et al. to characterize this propeller blade design theory, so this paper aims to design a global minimum torque propeller from scratch (referred by us as the *"Prandtl"* propeller) and compare this across all advance ratios to an equivalent MIL propeller. These blades would present with the same thrust, chord distribution, planform, airfoil distribution, and advance ratio design point. Therefore, the only difference between the MIL blade and our Prandtl blade is the blade twist (β) across r. Since the MIL design has been the standard for efficiency since its inception, this was chosen to be the baseline case for comparison. The methodology for design of the MIL propeller is based mainly off of Larrabee's work [6]. Although more studies have been conducted, such as one of particular interest out of Baylor [8, 9], the propeller design process and testing of the propeller were mainly focused on acoustic testing. This research effort has been aimed at the design process of a propeller with this optimized twist, the prediction methodology of the different steps of that process, and, in later work, the comparison of results of multiple differing-fidelity methodologies for efficiency predictions.

While the main objective of this research is to explore the possible increase in efficiency that can be attained using the Prandtl Bell Spanload design philosophy, acoustic benefits can also be seen as motivation for this study. There are plans currently in place to complete some acoustic testing in the NASA Langley Low-Speed Acoustic Wind Tunnel (LSAWT) that has been shown to produce promising results for similar propellers [10–12] in both size and performance parameters. The hypothesis that will be tested is that the noise generated could be reduced for the Prandtl blade due to the reduced loading on the tip of the blade [13, 14]. A similar approach has been shown to produce a reduced noise signature [15] with the tip of the propeller untwisted.

A large motivation for this research is the increasing amount of interest in the field of Urban Air Mobility (UAM) and its challenges [16]. The design and testing phase of UAM vehicles has been shown in previous research to be a complex systems engineering problem [17–19]. Two major challenges for widespread use of UAM vehicles are noise pollution and the vehicle efficiency. Since the largest contributor to noise and energy use of most UAM vehicles is the propulsion system, a new propeller design can be created to: (1) increase efficiency and (2) produce favorable acoustic behavior. These concepts are meant to fly in a populated area, so much of the propeller-based research currently conducted is focused on the acoustic side of these issues [20, 21]. The propeller design described in this paper is shown to be more efficient with the potential to be quieter as well.

III. Methodology

The design process for this classification of propeller starts first with the results of the optimization by Bowers et al. The results of their analysis showed an optimal C_l distribution that would minimize the torque while keeping the same thrust [4]. By considering the propeller in a three-dimensional sense, as opposed to the current minimum-induced loss formulation that is purely a two-dimensional solution, the loading can be shifted inboard and the efficiency increased.

This is characterized by Fig. 3 for an example airfoil.

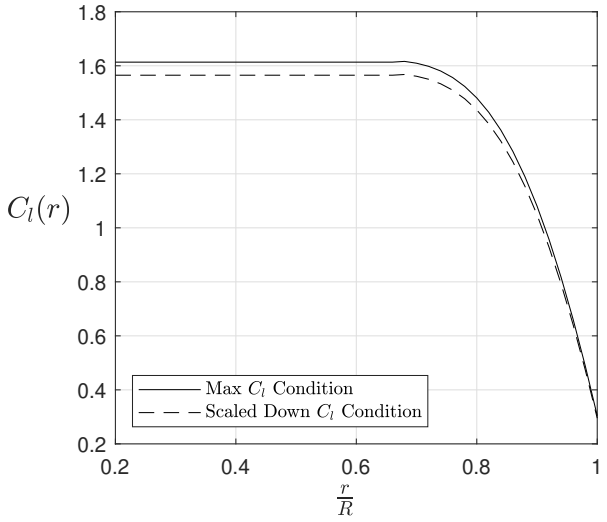

Fig. 3 Lift Coefficient Distribution for Example Airfoil

This redistribution of the loading leads to a reduced torque at the design point for the same thrust production. Although a true Prandtl propeller would follow the solid maximum lift coefficient line on Fig. 3 up until 72% r for the particular airfoil used, it is suggested that a small buffer of about 2% of C_l be added to account for uncertainty related to the airfoil polar generation as shown in the dashed line in Fig. 3. This is especially important on small propellers, where the Reynolds Number will be lower and the viscous forces more important.

A. Baseline Comparison

Since MIL has been utilized as the gold-standard for propeller design for a century, it was seen as a fitting comparison case. As was stated in the introduction, the process for this was based mainly off of Larrabee's work [6], which shows that the efficiency of the propeller as a whole is expressed by-

$$\eta = \frac{\int_0^1 \eta_e \frac{dT}{d\xi} d\xi}{T_c} \tag{1}$$

Where both η_e and $\frac{dT}{d\xi}$ are functions of ζ, which is characterized by-

$$\zeta = \frac{I_1}{2I_2}\left(1 - \sqrt{1 - \frac{4I_2 T_c}{I_1^2}}\right) \tag{2}$$

The terms I_1 and I_2 are then shown to be functions of G and the $\frac{D}{L}$ ratio-

$$I_1 = 4\int_0^1 G\left(1 - \frac{D/L}{x}\right)\xi d\xi \tag{3}$$

$$I_2 = 2\int_0^1 \frac{G\left(1 - \frac{D/L}{x}\right)\xi d\xi}{x^2 + 1} \tag{4}$$

G can be expressed as a function of Γ-

$$G = \frac{B\Omega\Gamma}{2\pi V v`} \tag{5}$$

Since G is a function of the operating point at each radial position, the $\frac{D}{L}$ ratio is the knob to turn at each section. Thus, each section was optimized using the maximum $\frac{L}{D}$. In doing this, the blade twist will be optimized in a two dimensional sense to be operating at the maximum thrust.

1. Comparison Criteria

After a design point is set, the torque can be defined as the ratio of power necessary for the propeller to spin at the RPM picked-

$$\tau = \frac{P}{\omega} \tag{6}$$

With a thrust goal and a torque estimate, two propellers can then be compared using non-dimensional coefficients and efficiencies based off of them.

$$C_T = \frac{T}{\rho n^2 D^4} \tag{7}$$

$$C_Q = \frac{Q}{\rho n^2 D^5} \tag{8}$$

$$C_P = \frac{2\pi n Q}{\rho n^3 D^5} \tag{9}$$

$$\eta_{dynamic} = J\frac{C_T}{C_P} \tag{10}$$

$$\eta_{static} = \frac{T^{3/2}}{2\pi n Q\sqrt{2\rho A}} \tag{11}$$

The use of Equations 7- 11 are essential to compare the Prandtl-designed propellers to the corresponding MIL propellers. To limit differences, everything was kept constant in the geometry except for the twist distribution.

B. Blade Twist Distribution Calculation

The β distribution is calculated by simply adding the two contributions to the blade twist: angle of attack (α) and resultant inflow angle (ϕ).

$$\beta = \alpha + \phi \tag{12}$$

Equation 12 takes the ϕ angle, characterized as the resultant inflow angle of the blade, and α, the local angle of attack. Since α is calculated at each section using the C_l distribution and the lift curve, ϕ is the remaining variable needed to compute β. This can be calculated using-

$$\phi = \arctan\left(\frac{V_0}{\omega r}\right) \tag{13}$$

Where V_0 is the free-stream velocity perpendicular to the rotational plane (in meters per second) and ω is the rotational velocity (in rotations per second) of the propeller. ϕ is then calculated across the blade span, r.

As an example, the design point for one of the propellers to be discussed in later sections is 3000 rotations per minute (RPM) with a free-stream velocity of 9.144 meters per second, corresponding to an advance ratio of 0.4. Thus the inflow angle can be visualized in Figure 4.

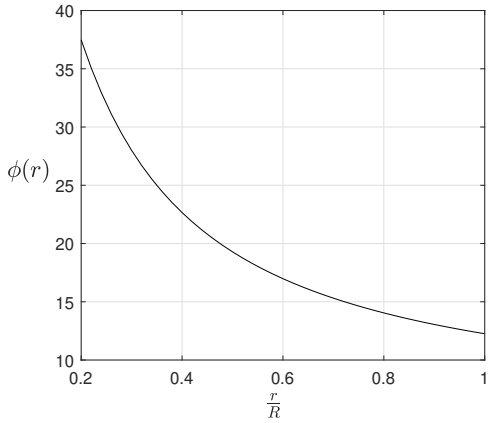

Fig. 4 Example Inflow Angle, ϕ, Along Blade Span

C. Airfoil Choice

The next key design consideration is the airfoil choice. Since this propeller is designed to operate near the maximum lift coefficient, it would be advantageous to pick an airfoil with favorable stall characteristics and whose $\frac{C_l}{C_{d\,max}}$ point is near the maximum C_l. For the inboard section, up to the 72% break-point, the two airfoils considered were the NACA 6412 and the MH 115. These airfoils were seen to fit the criteria listed above, with the NACA 6412 operating very near the $\frac{C_l}{C_{d\,max}}$ point and the MH 115 having favorable stall characteristics.

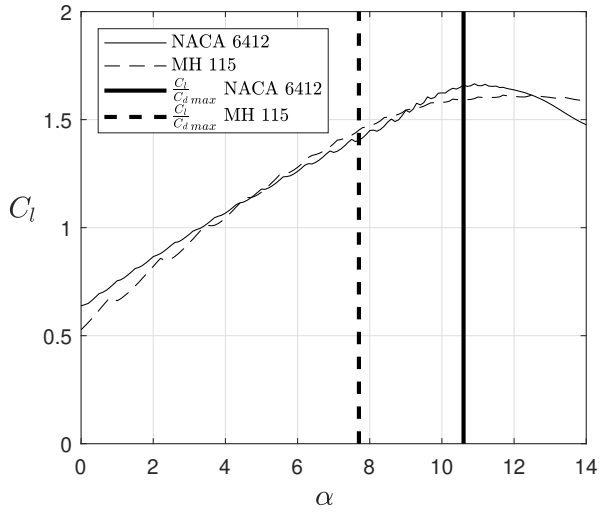

Fig. 5 Rectangular Chord Distribution XROTOR Geometry

These two airfoils are shown to be comparable as far as maximum lift coefficient, with about a 0.05 difference between the two, but the NACA 6412 is shown to have a steeper drop-off after the apex of the curve. The MH 115 is shown to qualitatively have better stall characteristics, as well as having a higher maximum lift to drag ratio, shown in Figure 6.

Figure 6 shows that, although the plots show a high degree of variance, the $\frac{C_l}{C_{d\,max}}$ of the NACA 6412 is below the MH 115 by a wide enough margin that it would be acceptable to assume this to be the case. A difference can be seen in both the shape of the plot and the location of the maximum, which is of particular importance. Although the location of the maximum $\frac{C_l}{C_{d\,max}}$ for the NACA 6412 is much closer to the maximum C_l, the actual values are very comparable

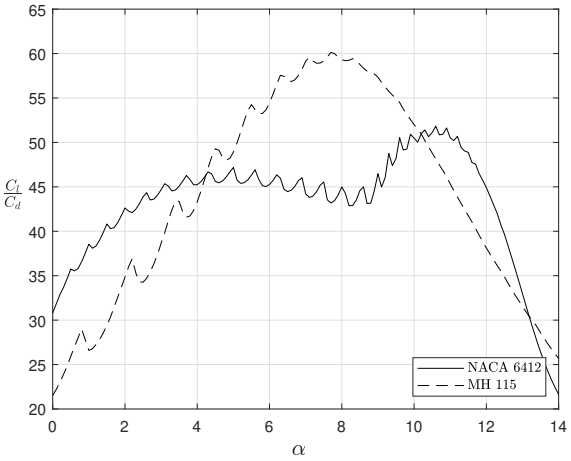

Fig. 6 Lift-to-Drag Ratio Curves

between airfoils, with the MH 115 operating at nearly the same lift-to-drag ratio at the NACA 6412's maximum point. This, along with the more favorable stall characteristics led to the choice of this airfoil to be used in this design.

Figure 6 shows the lift-to-drag ratio for each airfoil, a term of significance when considering the aerodynamics during the design phase. This term is also a major reason for the NACA-style airfoil to be under consideration, with the maximum value occurring at virtually an identical angle of attack as the maximum lift coefficient point. This is interesting and almost led to this airfoil being used going forward in the design process because this would benefit the novel design. However, when plotted on the same figure, it is seen that that the envelope of interest includes the area of the plot where the MH-115 presents with values higher or nearly the same to the NACA airfoil. An additional benefit is less variance on the MH-115 values for the higher angles of attack.

A quick check was completed on the Reynolds' Number to ensure previous assumptions are upheld for the local airfoil sections. The main assumption was that the Reynolds' Number was above $100,000$ at the 75% span location. This is in line with standard procedure to limit the unpredictability of this very low regime [22]. The specific number was found to be about 128,000, above the imposed limit and in the region of the XFOIL analysis conducted.

D. Blade Design Iterations

In order to explain the different design iterations performed to reach our final design, the following sections describe each consecutive design iteration and the reasoning behind the changes. For each design iteration, a Prandtl version and equivalent MIL version producing the same thrust with the same geometry *except* for the blade twist was created as a comparison.

1. Constant Chord and Constant Airfoil Distributions

To design an initial test case, an eighteen inch diameter propeller with a constant (i.e. rectangular) chord distribution and constant airfoil distribution was designed as a simplified starting point. In order to calculate the blade twist, V_0 was defined as 9.144 m/s and ω was defined as 50 revolutions per second (i.e. 3000 revolutions per minute). The chord length was then chosen to be based off of the chord length of two commercial off-the-shelf (COTS) propellers on-hand. The overall average of the chords of multiple COTS propellers of similar diameter was used as the single chord length across the blade span during the geometry design. This resulted in the following chord distribution-

Where the solid line in Fig. 7a is the designed chord and the dashed line is the minimum allowable chord (i.e the chord that gives a maximum lift coefficient at each point). Figure 7b shows the Bowers et al. C_l distribution (solid line) when it is applied to this constant chord and airfoil distribution as well as the max C_l possible (dashed line) across the blade span. Since the airfoil is constant in this iteration, the max C_l is also constant. From this, the β distribution can be calculated for each section as shown in the solid line in Fig. 8b which is compared to the MIL β distribution in the dashed line.

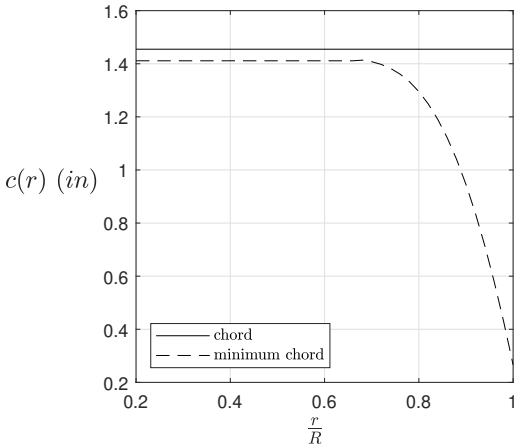

(a) Chord Design vs Minimum Chord

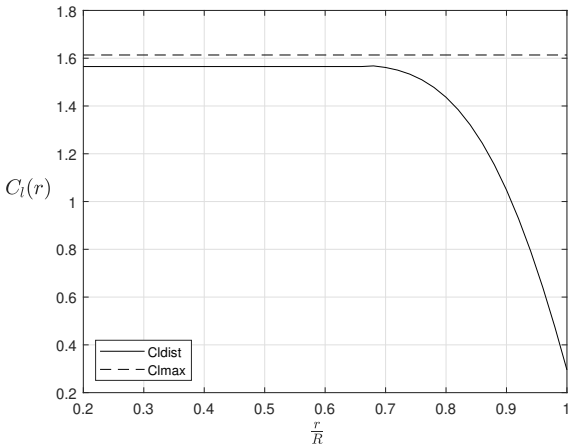

(b) C_l Design vs. $C_{l_{max}}$

Fig. 7 Rectangular Chord Distribution Blade Design Chord and C_l

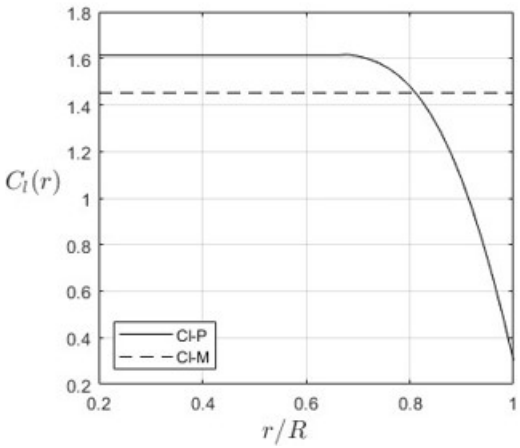

(a) Prandtl vs MIL C_l Comparison

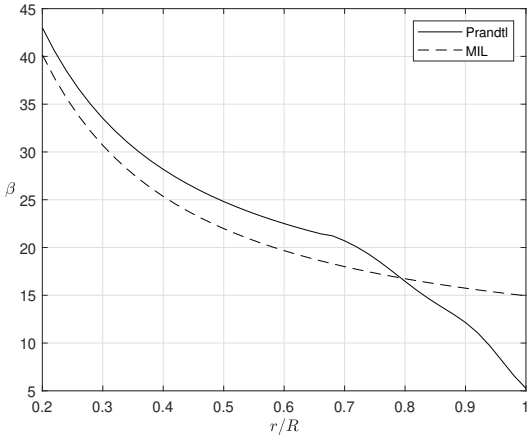

(b) Prandtl vs MIL β Comparison

Fig. 8 Rectangular Chord Distribution Blade Design C_l and β for Prandtl vs MIL

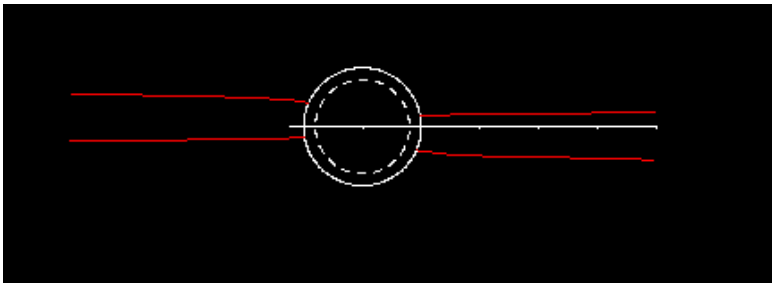

Fig. 9 Rectangular Chord Distribution XROTOR Geometry

Figure 9 shows the XROTOR generated geometry. This can then be run through the program for a set of point design results.

Table 1 Efficiency Predictions for Prandtl vs MIL Constant Chord and Airfoil Blade Geometry

$Propeller$	$Prandtl$	MIL
$Thrust$	12.7 N	13.1 N
$Torque$	0.598 Nm	0.637 Nm
C_T	0.0950	0.0981
C_P	0.0614	0.0653
$Efficiency(\eta)$	0.619	0.600

From the results in Table 1, the efficiency is seen to increase by *3.3*%. This is encouraging since MIL has been the gold standard for propeller design since it was introduced by Betz in the 1920s and widely considered to be the optimal propeller blade design solution [6].

2. Constant Chord with Non-constant Airfoil Distributions

As a next step in complexity, a new design can be created that changes airfoils across the span. The reasoning behind changing the airfoils is due to the Prandtl blade dumping a large amount of lift quickly on the outboard sections. The two ways to design this into the blade is with twist and airfoil change. For a constant airfoil blade, there will be a large amount of twist on the blade near the tip of the blade. By utilizing a more symmetric airfoil at the tip, some of this difference can be mitigated to decrease strain on the blade. There is also a balance that must be met between the twist and the airfoil. Although a quick change in twist can be almost completely mitigated through a large decrease in camber, this would increase the amount of space necessary for a smooth transition between airfoils. The airfoil distribution is thus changed to blend between the MH 115 to an S4310. This blend occurs between an $\frac{r}{R}$ of 0.72 and 0.98, respectively. Additionally, the blend was made nonlinear to more slowly change at the beginning of the range before dropping off. The S4310 drops the maximum lift coefficient by about 0.2 with comparable key locations on the polars, such as angle of maximum lift coefficient. Figure 10 visually shows the transition between the MH 115 and S4310 airfoils along the blade span: the blue section corresponds to the MH115, the green section corresponds to the non-linear transition between the MH 115 and S4310 airfoils, and the red section corresponds to the S4310.

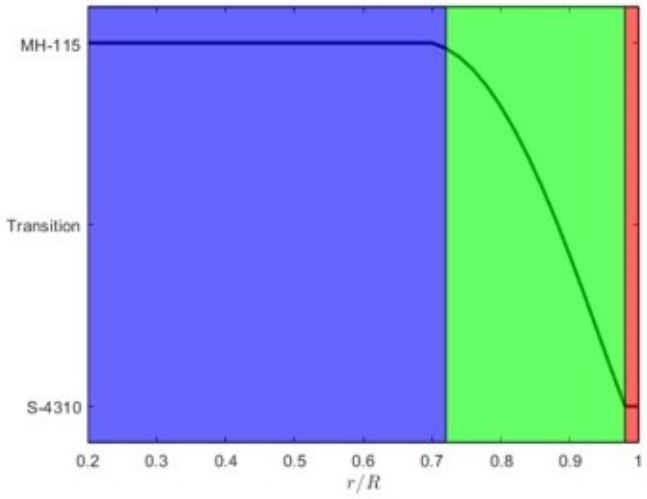

Fig. 10 Airfoil Non-linear Transition from MH 115 to S4310 Across Blade Span

The effect of the airfoil distribution can be seen by looking at the difference in the lift coefficient plots. The change in airfoil manifests as a slight decrease in maximum lift coefficient at the tip, shown on Fig. 11. In general, the lift

distribution necessary to produce the Prandtl Propeller allows for a large change in camber in the outboard section, leaving the practicality of the geometry as the main constraint. As such, a less aggressive airfoil change was utilized in this proof of concept design.

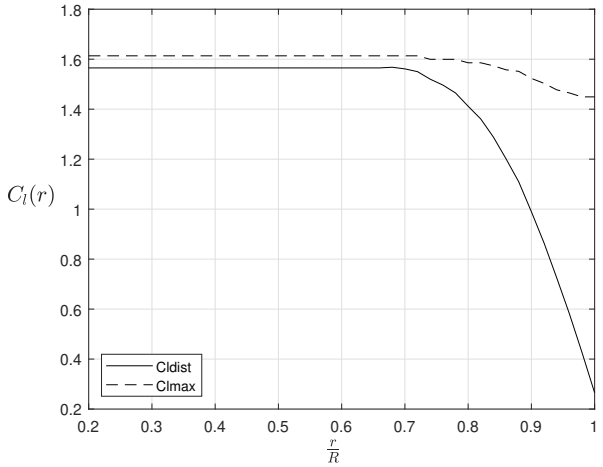

Fig. 11 C_l Distribution vs $C_{l_{max}}$ for Rectangular Chord Distribution with Non-constant Airfoil Distribution

The twist distribution in Fig. 12b is seen to slightly change, including slightly higher twist values at the tip, pointing towards a less aggressive twist change. This helps unload the tip more easily than purely untwisting a highly cambered airfoil and is the reasoning behind transitioning airfoils to a less cambered airfoil at the tip.

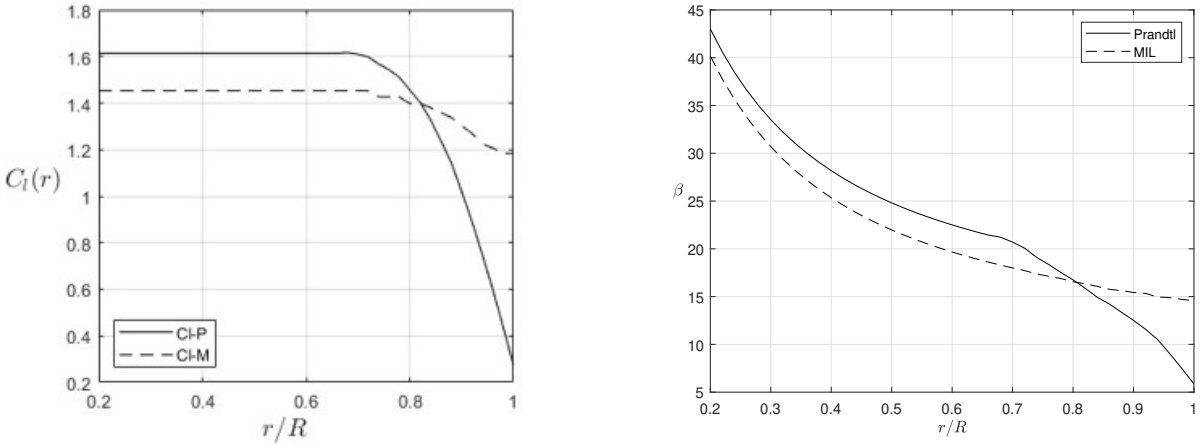

(a) Prandtl vs MIL C_l Comparison **(b) Prandtl vs MIL β Comparison**

Fig. 12 Rectangular Chord and Non-constant Airfoil Distribution Blade Design C_l and β for Prandtl vs MIL

From the results in Table 2, the efficiency is seen to increase by *2.9*% for an advance ratio of 0.4. Even though this is less of an increase than the constant airfoil blade in the previous section, it is believed that the less cambered airfoil at the tip will improve the acoustic performance.

3. Non-constant Chord and Non-constant Airfoil Distribution

After an airfoil change is applied, the next step in complexity is to design a blade that exhibits a non-rectangular chord. This opens up the design space and allows for more complex features to increase efficiency. While a more

Table 2 Efficiency Predictions for Prandtl vs MIL Constant Chord and Non-constant Airfoil Blade Geometry

Propeller	*Prandtl*	*MIL*
Thrust	14.3 *N*	14.3 *N*
Torque	0.681 *Nm*	0.700 *Nm*
C_T	0.106	0.106
C_P	0.0699	0.0718
$Efficiency(\eta)$	0.609	0.593

efficient planform could be designed, the main goal of this paper is to discuss the effect of the redistribution of lift in relation to the minimum induced loss propeller, so a full optimization effort of chord distribution was not performed. A constant (rectangular) chord distribution is also less structurally sound and would not accurately represent real propellers, so it was desired to have a non-constant chord for this proof-of-concept propeller blade.

The chosen chord was inspired by a basic propeller shape. There was no real basis behind the shape of the chord, with the main driving factor just being to create a shape that looks like a propeller and can be used to compare the two twist designs. The chord utilized for this design iteration is shown by Figure 13a.

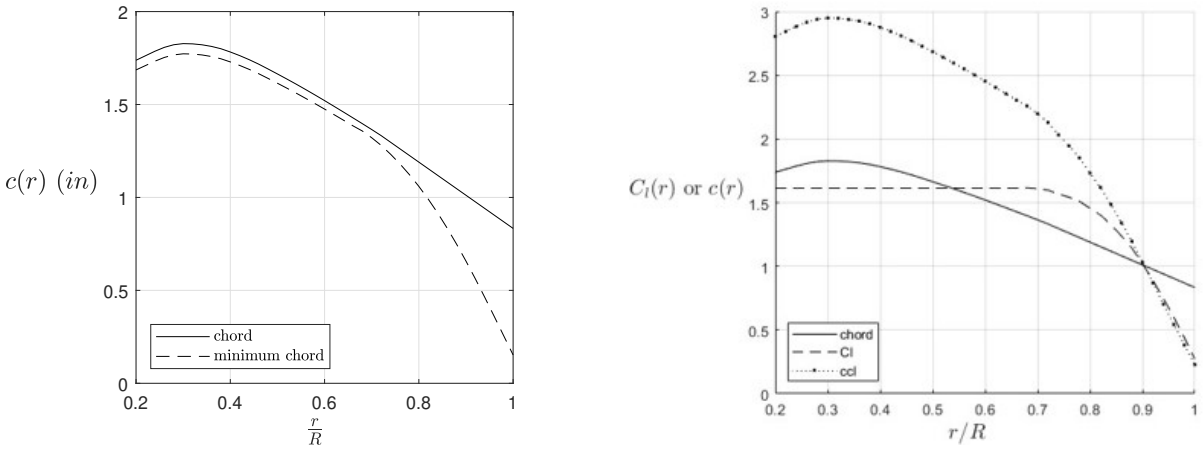

(a) Chord Distribution vs Minimum Chord Distribution

(b) Chord, C_l, and Lift (Chord*C_l) Distributions

Fig. 13 Non-constant Chord and Airfoil Distribution Blade Design Chord, C_l, and Lift (Chord*C_l)

For this blade, the airfoil distribution is kept the same as the last blade (non-constant airfoil distribution), and the new chord distribution shown in Fig. 13a is incorporated into the design. Additionally, since the lift coefficient is the design point for the Prandtl propeller, the angle of attack is the same between this and the last design. This leads both the $C_l(r)$ and $\beta(r)$ distributions to remain the same as well.

Table 3 Efficiency Predictions for Prandtl vs MIL Non-constant Chord and Airfoil Blade Geometry

Propeller	*Prandtl*	*MIL*
Thrust	19.4 *N*	19.8 *N*
Torque	1.02 *Nm*	0.98 *Nm*
C_T	0.145	0.148
C_P	0.101	0.104
$Efficiency(\eta)$	0.575	0.567

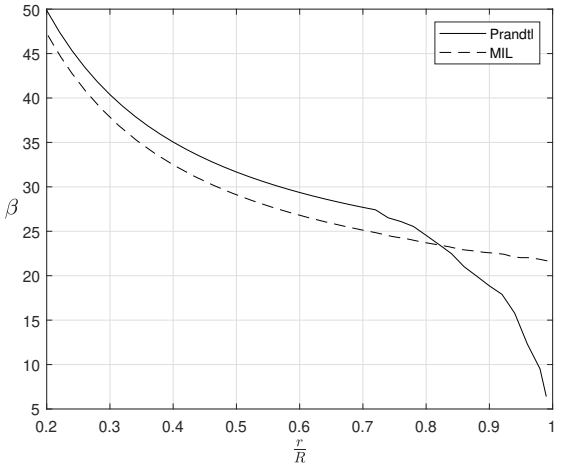

Fig. 14 β Distribution for the Final Design

From the results in Table 3, the efficiency is seen to increase by *2.0*%. The reduction in efficiency improvement between Prandtl and MIL for this design compared to the last design is accepted since a rectangular chord is impractical for real-world applications due to the higher stresses on the blade root and anticipated degradation in acoustic properties. Additionally, this reduction is possibly due to the optimization of the blade being completed for the rectangular planform case, as opposed to a blade with a non-constant chord distribution.

E. Prandtl, MIL, and Combination Blades

The finalized versions of the blades were then created using the CAD program CREO so the propeller system could be fully visualized. The primary difference readily seen in each blade is the tip location, where the optimized propeller presents with a much lower angle of attack than the MIL. Figure 15 can be used to show the tip difference on the two blades.

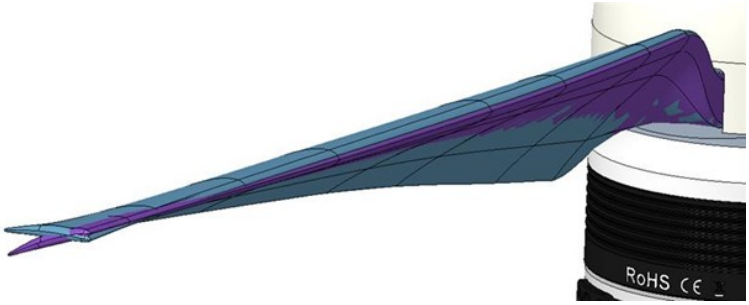

Fig. 15 CAD Models of Final Prandtl and MIL Blades - Front

In Figure 15, the Prandtl blade is colored in blue and the MIL is purple. This model is thus shown to exemplify the twist difference discussed in Figure 14. Additionally, the area closer to the root can be compared in Figure 16.

Since the "100%" Prandtl blade is maxed in its C_l for a good proportion of the blade span (max C_l up to 72% blade span), most of the blade is close to stall at its designed advance ratio. In order to design in some more robustness into the blade for operating at more advance ratios, combination blades blending MIL and Prandtl blade twists were also designed in order to determine the best trade-off between efficiency and operational robustness. These *"combo"* blades were designed for the final blade design with non-constant airfoil and chord distributions. This included using different percentages of the blade twist of each, allowing for blades that would be farther from a maximum lift coefficient condition (e.g. a 70% Prandtl and 30% MIL combo blade or "70-30" combo blade).

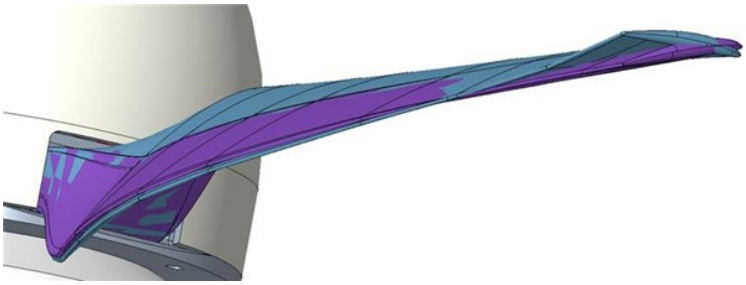

Fig. 16 CAD Models of Final Prandtl and MIL Blades - Back

The set of blades created starts at a "50-50" blade and incrementally increases the percentage of the Prandtl distribution by ten percent. An interesting and convenient comparison case can be drawn through the use of this strategy. The effect of slightly backing off the angle of attack in areas near the root and increasing the angle of attack at the tip can then be tested. The difference between each incremental difference can be most clearly seen in the tip region of the propellers, visualized in Figure 17.

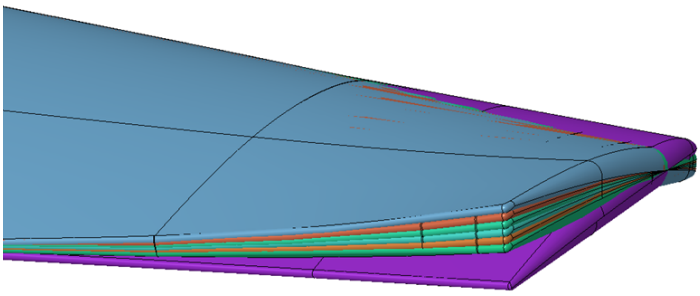

Fig. 17 Combination Blade Tip Twist Comparison

The blades, visualized in Figure 17, will provide additional context to the results in Section IV and show trends as the propellers transition between the two design philosophies.

IV. Results

With a final geometry in place, predictions can be made. These include the design point analysis, as well as C_P, C_T, C_Q, and η curves with respect to the advance ratio. The main prediction methodology used was the XROTOR code, by Mark Drela [23]. This program provides these terms as outputs, using the geometry and flight conditions as inputs. The drawback to utilizing this code is that the relatively simple framework, while still very powerful, is limited. The viscous effects are very input dependent and iteration is necessary to ensure the drag values for each aerodynamic slice are accurate given the Reynolds Number on the airfoil cross-section. Additionally, there is an acoustic solver, although a more refined solver would be be sought out for any prediction methodology to be conducted later.

A. XROTOR Analysis

The XROTOR analysis was conducted on input files, including the one housed within Appendix B. This input file is that of the Prandtl inspried blade, which constitutes Figures 18 and 19. These plots show the behavior of the propeller over the entire advance ratio sweep, with line of constant RPM used to show that behavior.

Although a large RPM range is utilized, the results for the C_P and C_T are particularly close. The 8000 RPM line is shown to set itself apart slightly from the rest, which are almost identical to each other. The efficiency curve, however,

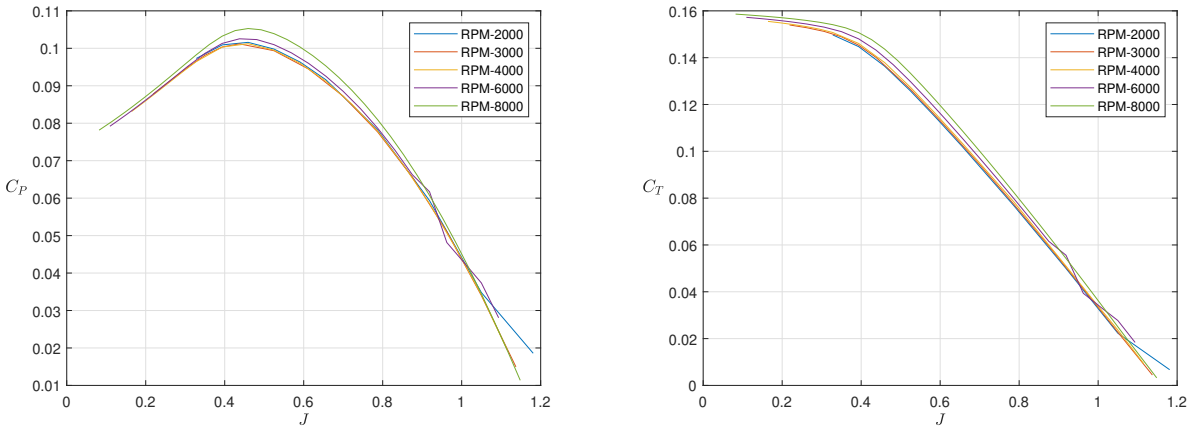

(a) C_P Curve for All Tested RPMs **(b) C_T Curve for All Tested RPMs**

Fig. 18 C_P and C_T Curves for the Prandtl Blade

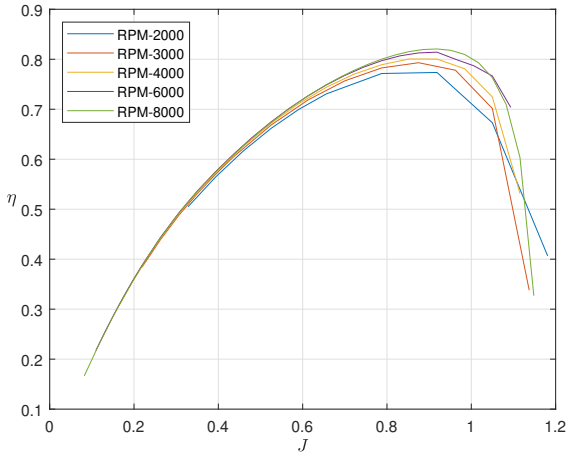

Fig. 19 Prandtl Blade RPM Sweep Efficiency Results

shows more difference, especially at higher advance ratios. For lower values, there is not much change between RPM lines before the difference grows and the curves becomes more erratic. After this, a comparison can be drawn between every propeller at the 3000 RPM point, the closest to the specific point that the propellers were designed around. This is shown in Figures 20a- 21.

Figure 20a shows some interesting behavior near the beginning of the curve. The MIL designed blade seems to have a more parabolic shape, while the Prandtl blade has a much sharper incline in that same area. Additionally, every plot features a peak in the general vicinity of the advance ratio of 0.4 point. Figure 20b displays fairly linear behavior for most of the C_T curve, with the exception of points occurring before ≈ 0.4 on the advance ratio sweep. When reviewing the efficiency sweep, Figure 21, the Prandtl propeller and all of the intermediate blade results are nearly identical. However, the most interesting part of this plot is that there is a gap seen between these blades and the MIL designed blade. Although very close, a visible difference can be seen from advance ratios of 0.45-1.05.

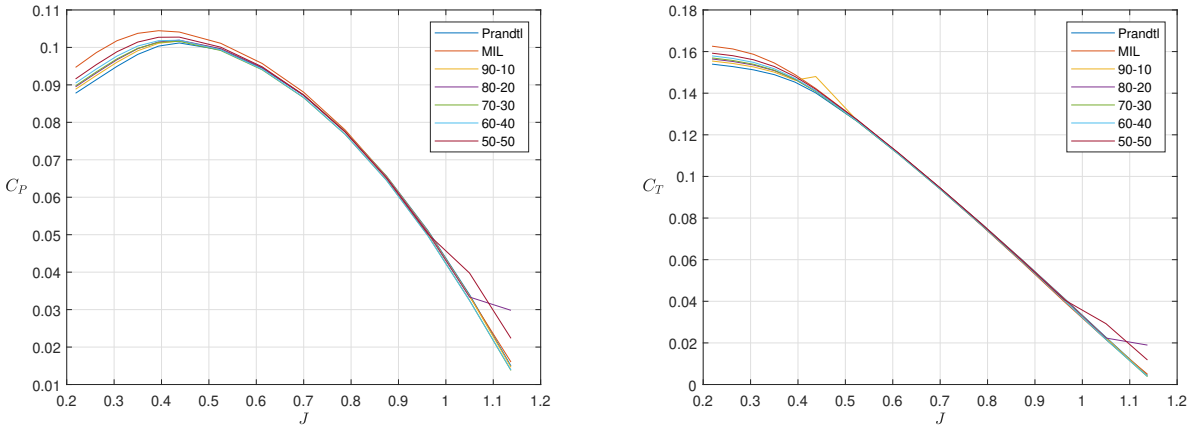

(a) C_P Curve Comparison for All Blades **(b) C_T Curve Comparison for All Blades**

Fig. 20 C_P and C_T Curve Comparison at 3000 RPM

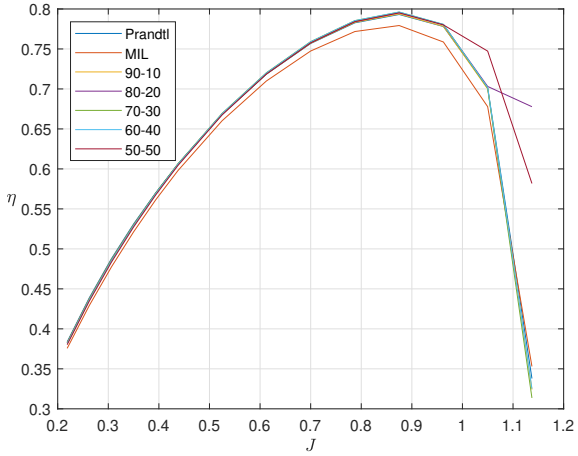

Fig. 21 Efficiency Comparison for All Blades at 3000 RPM

V. Conclusion

The Prandtl Bell wing span-load has been investigated as an improvement over the traditional elliptical wing span-load due to it's unloading of the wingtip allowing for favorable structural, aeronautic, and acoustic properties [1]. A small section of the Bowers et al. 2021 paper on the experimental test of a wing with the Bell span-load described the formulation of a propeller using a similar thought process [4]. Bowers et al. described an optimization algorithm which optimizes for global torque across a propeller blade and is the full three dimensional solution for minimizing torque. This is unlike the traditional propeller blade design theory, minimum induced loss (MIL), which is only a two dimensional solution for each cross-section of a blade.

In order to further test this idea as a proof-of-concept, this study aimed to design a novel *"Prandtl"* propeller which has the C_l distribution found by Bowers et al.'s optimization algorithm as well as an equivalent MIL blade with the same geometry as the Prandtl blade except for the twist and analyze their performance. Future work will involve experimentally testing the blades in a wind tunnel and acoustic anechoic chamber in order to verify the analysis. The airfoil distribution, chord distribution, and advance ratio design point were all evaluated to make a final design of the novel Prandtl and baseline MIL blades for comparison between each other. Combination blades were also designed in order to determine the optimal trade-off between efficiency, robustness, and acoustics.

XROTOR analysis of all the propeller design iterations have shown an increase in efficiency of 2.0-3.3% of the Prandtl blade when compared to an equivalent MIL blade. This is significant because the MIL blade theory has been the gold standard for propeller blade efficiency since the 1920's [5, 6] and is widely believed to be the most efficient a propeller blade can be. These results give some confidence that this design philosophy can be utilized to create a propeller that has a higher efficiency value. Additionally, it is thought there is a possible acoustic benefit attributed to the loading difference between blades. However, this assertion has yet to be tested and is only speculated.

Prandtl, MIL, and combination propeller blades have been generated in CAD and are planned to be fabricated and tested in the Low-Speed Anechoic Wind Tunnel (LSAWT) at NASA Langley. This will provide experimental efficiency and acoustic data across the full operational advance ratio range to validate the analysis which shows promising results for these propeller designs. This is an initial proof-of-concept study, and these propeller designs can be picked up by academia and industry to further refine their characteristics and use them in real-world applications to improve propeller flight. Academia, industry, and Government are actively working towards a future where dozens of small to large Unmanned Aerial Systems (UAS) are present within urban environments. In this environment, high noise pollution and inefficiencies have the potential to render these new technologies impractical due to public annoyance and nonacceptance. Two major breakthroughs for enabling widespread use of UAS in urban environments are noise reduction and vehicle efficiency, and this new propeller design promises to provide both.

References

[1] Bowers, A. H., Murillo, O. J., Jensen, R. R., Eslinger, B., and Gelzer, C., "On Wings of the Minimum Induced Drag: Spanload Implications for Aircraft and Birds," 2016.

[2] Robb, C., and Paul, R., "Aerodynamic Modeling of a Flying Wing Featuring Ludwig Prandtl's Bell Spanload," *Aerospace*, Vol. 10, No. 7, 2023, p. 613.

[3] Robb, C. S., Vuppala, R. K., Paul, R. C., and Kara, K., "Flight Dynamics of a Flying Wing Aircraft Featuring the Bell Spanload," *AIAA SCITECH 2023 Forum*, 2023, p. 2610.

[4] Bowers, A. H., Murillo, O. J., Berger, D. E., Hawkins, V. S., Newton, L. J., Waddell, A. G., Glover, E. D., Brady, J. C., Bodylski, J. K., Bowers, R. A., et al., "Experimental Flight Validation of the Prandtl 1933 Bell Spanload," 2021.

[5] Betz, A., "Airscrews with minimum energy loss," *Report, Kaiser Wilhelm Institute for Flow Research*, 1919.

[6] Larrabee, E. E., "Practical design of minimum induced loss propellers," *SAE Transactions*, 1979, pp. 2053–2062.

[7] Marte, J. E., and Kurtz, D. W., "A Review of Aerodynamic Noise From Propellers, Rotors, and Lift Fans," 1970.

[8] Van Treuren, K. W., Sanchez, R., Bennett, B., and Wisniewski, C., "Design of Propellers for Minimum Induced Drag," *AIAA AVIATION 2021 FORUM*, 2021, p. 2225.

[9] Van Treuren, K. W., Sanchez, R., Bennett, B., and Wisniewski, C., "Testing UAS Propellers Designed for Minimum Induced Drag," *AIAA AVIATION 2021 FORUM*, 2021, p. 2221.

[10] Zawodny, N. S., Boyd Jr, D. D., and Burley, C. L., "Acoustic characterization and prediction of representative, small-scale rotary-wing unmanned aircraft system components," *American Helicopter Society (AHS) Annual Forum*, 2016.

[11] Ingraham, D., "Low-Noise Propeller Design with the Vortex Lattice Method and Gradient-Based Optimization," *AIAA SCITECH 2023 Forum*, 2023, p. 2039.

[12] Zawodny, N. S., and Haskin, H., "Small propeller and rotor testing capabilities of the NASA Langley Low Speed Aeroacoustic Wind Tunnel," *23rd AIAA/CEAS Aeroacoustics Conference*, 2017, p. 3709.

[13] Hanson, L. P., Baskaran, K., Pullin, S. F., Zhou, B. Y., Zang, B., and Azarpeyvand, M., "Aeroacoustic and Aerodynamic Characteristics of Propeller Tip Geometries," *28th AIAA/CEAS Aeroacoustics 2022 Conference*, 2022, p. 3075.

[14] Wisniewski, C. F., "Effect of Varying Propeller Pitch Angle on Efficiency and Noise Production," *AIAA Scitech 2021 Forum*, 2021, p. 0613.

[15] Ghoreyshi, M., Aref, P., Wisniewski, C. F., Seidel, J., and Van Treuren, K. W., "Computational investigation of quiet propeller designs for small unmanned aerial vehicles," *Aerospace Science and Technology*, 2023, p. 108351.

[16] Rizzi, S. A., Huff, D. L., Boyd, D. D., Bent, P., Henderson, B. S., Pascioni, K. A., Sargent, D. C., Josephson, D. L., Marsan, M., He, H. B., et al., "Urban air mobility noise: Current practice, gaps, and recommendations," Tech. rep., 2020.

[17] North, D. D., Busan, R. C., and Howland, G., "Design and Fabrication of the LA-8 Distributed Electric Propulsion VTOL Testbed," *AIAA SciTech 2021 Forum*, 2021, p. 1188.

[18] Button, K., "For Vahana, a study in coping with complexity," *AEROSPACE AMERICA*, Vol. 57, No. 6, 2019, pp. 14–19.

[19] Murphy, P. C., and Landman, D., "Experiment design for complex VTOL aircraft with distributed propulsion and tilt wing," *AIAA Atmospheric Flight Mechanics Conference*, 2015, p. 0017.

[20] Pinto, O. L., Bossotto, G., Afonso, F., and Lau, F., "On Rotor Aeroacoustic Optimization for Urban Air Mobility," *28th AIAA/CEAS Aeroacoustics 2022 Conference*, 2022, p. 2946.

[21] Christian, A. W., and Cabell, R., "Initial investigation into the psychoacoustic properties of small unmanned aerial system noise," *23rd AIAA/CEAS aeroacoustics conference*, 2017, p. 4051.

[22] Deters, R. W., Ananda Krishnan, G. K., and Selig, M. S., "Reynolds number effects on the performance of small-scale propellers," *32nd AIAA applied aerodynamics conference*, 2014, p. 2151.

[23] Drela, Mark and Youngren, Harold, "XROTOR," , 2003. URL `http://web.mit.edu/drela/Public/web/xrotor/xrotor_doc.txt`.

A. Novel Prandtl and Baseline MIL Propeller Geometries

Table 4 Full Geometry of 18in Diameter Novel Prandtl Propeller

r/R	c/R	$r[in]$	$c[in]$	$Airfoil$	$Twist(\beta)$
0.2000	0.1931	1.80	1.738	$MH115$	49.52
0.2200	0.1958	1.98	1.762	$MH115$	47.52
0.2400	0.1985	2.16	1.787	$MH115$	45.58
0.2600	0.2008	2.34	1.807	$MH115$	43.74
0.2800	0.2024	2.52	1.822	$MH115$	42.02
0.3000	0.2031	2.70	1.828	$MH115$	40.45
0.3200	0.2029	2.88	1.826	$MH115$	39.04
0.3400	0.2024	3.06	1.821	$MH115$	37.77
0.3600	0.2014	3.24	1.813	$MH115$	36.65
0.3800	0.2000	3.42	1.800	$MH115$	35.67
0.4000	0.1981	3.60	1.783	$MH115$	34.81
0.4200	0.1959	3.78	1.763	$MH115$	34.06
0.4400	0.1935	3.96	1.741	$MH115$	33.40
0.4600	0.1908	4.14	1.717	$MH115$	32.81
0.4800	0.1879	4.32	1.691	$MH115$	32.28
0.5000	0.1849	4.50	1.664	$MH115$	31.80
0.5200	0.1819	4.68	1.637	$MH115$	31.34
0.5400	0.1788	4.86	1.609	$MH115$	30.90
0.5600	0.1756	5.04	1.580	$MH115$	30.47
0.5800	0.1723	5.22	1.551	$MH115$	30.04
0.6000	0.1690	5.40	1.521	$MH115$	29.61
0.6200	0.1656	5.58	1.490	$MH115$	29.16
0.6400	0.1622	5.76	1.460	$MH115$	28.71
0.6800	0.1552	6.12	1.397	$MH115$	27.77
0.7000	0.1517	6.30	1.365	$MH115$	27.28
0.7200	0.1481	6.48	1.333	$MH115$	26.77
0.7400	0.1441	6.66	1.297	$A3$	26.25
0.7600	0.1401	6.84	1.261	$A3$	25.70
0.7800	0.1362	7.02	1.226	$A3$	25.12
0.8000	0.1322	7.20	1.190	$A4$	24.48
0.8200	0.1283	7.38	1.154	$A4$	23.77
0.8600	0.1203	7.74	1.083	$A6$	21.97
0.8800	0.1164	7.92	1.047	$A7$	20.78
0.9100	0.1104	8.19	0.994	$A11$	18.44
0.9494	0.1026	8.54	0.924	$A13$	13.85
0.9786	0.0968	8.81	0.872	$s4310$	8.81
0.9997	0.0927	9.00	0.834	$s4310$	3.99

Table 5 Full Geometry of 18in Diameter MIL (Baseline) Propeller

r/R	c/R	$r[in]$	$c[in]$	$Airfoil$	$Twist(\beta)$
0.2000	0.1931	1.800	1.738	MH 115	47.25
0.2200	0.1958	1.980	1.762	MH 115	44.91
0.2400	0.1985	2.160	1.787	MH 115	42.82
0.2600	0.2008	2.340	1.807	MH 115	40.97
0.2800	0.2024	2.520	1.822	MH 115	39.32
0.3000	0.2031	2.700	1.828	MH 115	37.84
0.3200	0.2029	2.880	1.826	MH 115	36.52
0.3400	0.2024	3.060	1.821	MH 115	35.34
0.3600	0.2014	3.240	1.813	MH 115	34.28
0.3800	0.2000	3.420	1.800	MH 115	33.33
0.4000	0.1981	3.600	1.783	MH 115	32.46
0.4200	0.1959	3.780	1.763	MH 115	31.67
0.4400	0.1935	3.960	1.741	MH 115	30.95
0.4600	0.1908	4.140	1.717	MH 115	30.29
0.4800	0.1879	4.320	1.691	MH 115	29.69
0.5000	0.1849	4.500	1.664	MH 115	29.12
0.5200	0.1819	4.680	1.637	MH 115	28.60
0.5400	0.1788	4.860	1.609	MH 115	28.11
0.5600	0.1756	5.040	1.580	MH 115	27.65
0.5800	0.1723	5.220	1.551	MH 115	27.23
0.6000	0.1690	5.400	1.521	MH 115	26.82
0.6200	0.1656	5.580	1.490	MH 115	26.44
0.6400	0.1622	5.760	1.460	MH 115	26.07
0.6800	0.1552	6.120	1.397	MH 115	25.40
0.7000	0.1517	6.300	1.365	MH 115	25.08
0.7200	0.1481	6.480	1.333	MH 115	24.79
0.7400	0.1441	6.660	1.297	A3	24.50
0.7600	0.1401	6.840	1.261	A3	24.22
0.7800	0.1362	7.020	1.226	A3	23.96
0.8000	0.1322	7.200	1.190	A4	23.71
0.8200	0.1283	7.380	1.154	A4	23.46
0.8600	0.1203	7.740	1.083	A6	23.00
0.8800	0.1164	7.920	1.047	A7	22.78
0.9494	0.1026	8.545	0.924	A13	22.07
0.9786	0.0968	8.807	0.872	s4310	21.80
0.9997	0.0927	8.997	0.834	s4310	21.61

Table 6 Airfoil Geometries

A3		A4		A6		A7		A11		A13	
X	Y	X	Y	X	Y	X	Y	X	Y	X	Y
1.0000	0.0013	1.0000	0.0013	1.0000	0.0013	1.0000	0.0013	1.0000	0.0013	1.0000	0.0013
0.9994	0.0015	0.9994	0.0015	0.9994	0.0015	0.9994	0.0015	0.9994	0.0014	0.9994	0.0014
0.9977	0.0021	0.9977	0.0021	0.9977	0.0020	0.9977	0.0020	0.9977	0.0018	0.9977	0.0018
0.9948	0.0031	0.9948	0.0030	0.9948	0.0029	0.9948	0.0028	0.9948	0.0025	0.9948	0.0024
0.9907	0.0044	0.9907	0.0043	0.9907	0.0041	0.9907	0.0039	0.9907	0.0035	0.9907	0.0032
0.9855	0.0061	0.9855	0.0059	0.9855	0.0056	0.9855	0.0054	0.9855	0.0047	0.9855	0.0043
0.9791	0.0082	0.9791	0.0079	0.9791	0.0074	0.9791	0.0071	0.9791	0.0061	0.9791	0.0056
0.9717	0.0106	0.9717	0.0102	0.9717	0.0095	0.9717	0.0092	0.9717	0.0078	0.9717	0.0071
0.9631	0.0133	0.9631	0.0128	0.9631	0.0120	0.9631	0.0115	0.9631	0.0097	0.9631	0.0088
0.9534	0.0163	0.9534	0.0157	0.9534	0.0146	0.9534	0.0141	0.9534	0.0119	0.9534	0.0108
0.9427	0.0196	0.9427	0.0189	0.9427	0.0176	0.9427	0.0169	0.9427	0.0142	0.9427	0.0129
0.9310	0.0231	0.9310	0.0223	0.9310	0.0207	0.9310	0.0199	0.9310	0.0167	0.9310	0.0151
0.9182	0.0269	0.9182	0.0259	0.9182	0.0241	0.9182	0.0231	0.9182	0.0194	0.9182	0.0175
0.9045	0.0308	0.9045	0.0298	0.9045	0.0276	0.9045	0.0265	0.9045	0.0222	0.9045	0.0201
0.8898	0.0350	0.8898	0.0337	0.8898	0.0313	0.8898	0.0301	0.8898	0.0252	0.8898	0.0227
0.8743	0.0392	0.8743	0.0379	0.8743	0.0351	0.8743	0.0337	0.8743	0.0282	0.8743	0.0255
0.8578	0.0436	0.8578	0.0421	0.8578	0.0390	0.8578	0.0375	0.8578	0.0314	0.8578	0.0284
0.8405	0.0481	0.8405	0.0464	0.8405	0.0430	0.8405	0.0414	0.8405	0.0346	0.8405	0.0313
0.8224	0.0526	0.8224	0.0508	0.8224	0.0471	0.8224	0.0453	0.8224	0.0379	0.8224	0.0343
0.8036	0.0572	0.8036	0.0552	0.8036	0.0512	0.8036	0.0492	0.8036	0.0413	0.8036	0.0373
0.7840	0.0617	0.7840	0.0596	0.7840	0.0553	0.7840	0.0531	0.7840	0.0446	0.7840	0.0403
0.7638	0.0662	0.7638	0.0639	0.7638	0.0594	0.7638	0.0571	0.7638	0.0479	0.7638	0.0433
0.7430	0.0707	0.7430	0.0682	0.7430	0.0634	0.7430	0.0609	0.7430	0.0512	0.7430	0.0463
0.7216	0.0751	0.7216	0.0725	0.7216	0.0673	0.7216	0.0648	0.7216	0.0545	0.7216	0.0493
0.6997	0.0793	0.6997	0.0766	0.6997	0.0712	0.6997	0.0685	0.6997	0.0577	0.6997	0.0523
0.6773	0.0835	0.6773	0.0806	0.6773	0.0750	0.6773	0.0721	0.6773	0.0608	0.6773	0.0552
0.6545	0.0874	0.6545	0.0844	0.6545	0.0785	0.6545	0.0756	0.6545	0.0638	0.6545	0.0579
0.6314	0.0912	0.6314	0.0881	0.6314	0.0820	0.6314	0.0790	0.6314	0.0668	0.6314	0.0607
0.6079	0.0947	0.6079	0.0916	0.6079	0.0853	0.6079	0.0821	0.6079	0.0695	0.6079	0.0632
0.5842	0.0981	0.5842	0.0949	0.5842	0.0884	0.5842	0.0851	0.5842	0.0722	0.5842	0.0657
0.5603	0.1011	0.5603	0.0978	0.5603	0.0912	0.5603	0.0879	0.5603	0.0746	0.5603	0.0680
0.5362	0.1040	0.5362	0.1007	0.5362	0.0939	0.5362	0.0905	0.5362	0.0769	0.5362	0.0702
0.5121	0.1065	0.5121	0.1031	0.5121	0.0962	0.5121	0.0928	0.5121	0.0790	0.5121	0.0721
0.4879	0.1089	0.4879	0.1054	0.4879	0.0984	0.4879	0.0949	0.4879	0.0809	0.4879	0.0739
0.4638	0.1107	0.4638	0.1072	0.4638	0.1002	0.4638	0.0966	0.4638	0.0826	0.4638	0.0755
0.4397	0.1124	0.4397	0.1089	0.4397	0.1018	0.4397	0.0982	0.4397	0.0840	0.4397	0.0769
0.4158	0.1136	0.4158	0.1101	0.4158	0.1030	0.4158	0.0994	0.4158	0.0852	0.4158	0.0781
0.3921	0.1146	0.3921	0.1110	0.3921	0.1039	0.3921	0.1003	0.3921	0.0861	0.3921	0.0790
0.3686	0.1147	0.3686	0.1112	0.3686	0.1042	0.3686	0.1007	0.3686	0.0866	0.3686	0.0795
0.3455	0.1147	0.3455	0.1112	0.3455	0.1042	0.3455	0.1007	0.3455	0.0868	0.3455	0.0798
0.3227	0.1138	0.3227	0.1104	0.3227	0.1036	0.3227	0.1002	0.3227	0.0866	0.3227	0.0797
0.3003	0.1127	0.3003	0.1094	0.3003	0.1027	0.3003	0.0994	0.3003	0.0861	0.3003	0.0794

A3		A4		A6		A7		A11		A13	
X	Y	X	Y	X	Y	X	Y	X	Y	X	Y
0.2784	0.1109	0.2784	0.1076	0.2784	0.1012	0.2784	0.0980	0.2784	0.0851	0.2784	0.0786
0.2570	0.1088	0.2570	0.1057	0.2570	0.0994	0.2570	0.0963	0.2570	0.0839	0.2570	0.0776
0.2362	0.1060	0.2362	0.1031	0.2362	0.0971	0.2362	0.0941	0.2362	0.0822	0.2362	0.0763
0.2160	0.1031	0.2160	0.1002	0.2160	0.0945	0.2160	0.0917	0.2160	0.0803	0.2160	0.0746
0.1964	0.0995	0.1964	0.0968	0.1964	0.0914	0.1964	0.0888	0.1964	0.0780	0.1964	0.0726
0.1776	0.0958	0.1776	0.0932	0.1776	0.0882	0.1776	0.0856	0.1776	0.0755	0.1776	0.0704
0.1595	0.0915	0.1595	0.0892	0.1595	0.0844	0.1595	0.0821	0.1595	0.0726	0.1595	0.0678
0.1422	0.0872	0.1422	0.0849	0.1422	0.0805	0.1422	0.0783	0.1422	0.0695	0.1422	0.0651
0.1257	0.0824	0.1257	0.0804	0.1257	0.0763	0.1257	0.0742	0.1257	0.0661	0.1257	0.0620
0.1102	0.0775	0.1102	0.0756	0.1102	0.0719	0.1102	0.0700	0.1102	0.0625	0.1102	0.0588
0.0955	0.0722	0.0955	0.0705	0.0955	0.0671	0.0955	0.0654	0.0955	0.0587	0.0955	0.0553
0.0818	0.0668	0.0818	0.0653	0.0818	0.0623	0.0818	0.0608	0.0818	0.0547	0.0818	0.0516
0.0690	0.0613	0.0690	0.0600	0.0690	0.0573	0.0690	0.0559	0.0690	0.0505	0.0690	0.0478
0.0573	0.0557	0.0573	0.0545	0.0573	0.0521	0.0573	0.0510	0.0573	0.0462	0.0573	0.0438
0.0466	0.0501	0.0466	0.0491	0.0466	0.0470	0.0466	0.0460	0.0466	0.0418	0.0466	0.0398
0.0369	0.0445	0.0369	0.0436	0.0369	0.0418	0.0369	0.0409	0.0369	0.0373	0.0369	0.0356
0.0283	0.0390	0.0283	0.0382	0.0283	0.0367	0.0283	0.0359	0.0283	0.0329	0.0283	0.0313
0.0209	0.0334	0.0209	0.0328	0.0209	0.0315	0.0209	0.0308	0.0209	0.0283	0.0209	0.0270
0.0145	0.0282	0.0145	0.0277	0.0145	0.0266	0.0145	0.0260	0.0145	0.0238	0.0145	0.0227
0.0093	0.0228	0.0093	0.0223	0.0093	0.0214	0.0093	0.0210	0.0093	0.0192	0.0093	0.0183
0.0052	0.0181	0.0052	0.0177	0.0052	0.0169	0.0052	0.0165	0.0052	0.0148	0.0052	0.0140
0.0023	0.0132	0.0023	0.0129	0.0023	0.0122	0.0023	0.0118	0.0023	0.0103	0.0023	0.0096
0.0006	0.0099	0.0006	0.0095	0.0006	0.0086	0.0006	0.0082	0.0006	0.0065	0.0006	0.0056
0.0000	0.0000	0.0000	0.0000	0.0000	0.0000	0.0000	0.0000	0.0000	0.0000	0.0000	0.0000
0.0006	-0.0011	0.0006	-0.0013	0.0006	-0.0018	0.0006	-0.0021	0.0006	-0.0030	0.0006	-0.0035
0.0023	-0.0034	0.0023	-0.0038	0.0023	-0.0046	0.0023	-0.0049	0.0023	-0.0064	0.0023	-0.0072
0.0052	-0.0068	0.0052	-0.0072	0.0052	-0.0081	0.0052	-0.0085	0.0052	-0.0101	0.0052	-0.0110
0.0093	-0.0104	0.0093	-0.0108	0.0093	-0.0117	0.0093	-0.0121	0.0093	-0.0138	0.0093	-0.0147
0.0145	-0.0129	0.0145	-0.0134	0.0145	-0.0145	0.0145	-0.0150	0.0145	-0.0170	0.0145	-0.0181
0.0209	-0.0156	0.0209	-0.0162	0.0209	-0.0173	0.0209	-0.0179	0.0209	-0.0202	0.0209	-0.0213
0.0283	-0.0173	0.0283	-0.0180	0.0283	-0.0194	0.0283	-0.0201	0.0283	-0.0228	0.0283	-0.0242
0.0369	-0.0192	0.0369	-0.0199	0.0369	-0.0215	0.0369	-0.0223	0.0369	-0.0254	0.0369	-0.0270
0.0466	-0.0201	0.0466	-0.0210	0.0466	-0.0229	0.0466	-0.0238	0.0466	-0.0276	0.0466	-0.0294
0.0573	-0.0211	0.0573	-0.0221	0.0573	-0.0243	0.0573	-0.0253	0.0573	-0.0296	0.0573	-0.0317
0.0690	-0.0214	0.0690	-0.0227	0.0690	-0.0251	0.0690	-0.0264	0.0690	-0.0313	0.0690	-0.0337
0.0818	-0.0216	0.0818	-0.0230	0.0818	-0.0258	0.0818	-0.0272	0.0818	-0.0328	0.0818	-0.0356
0.0955	-0.0214	0.0955	-0.0230	0.0955	-0.0261	0.0955	-0.0277	0.0955	-0.0340	0.0955	-0.0371
0.1102	-0.0210	0.1102	-0.0227	0.1102	-0.0262	0.1102	-0.0280	0.1102	-0.0349	0.1102	-0.0384
0.1257	-0.0203	0.1257	-0.0222	0.1257	-0.0261	0.1257	-0.0280	0.1257	-0.0357	0.1257	-0.0395
0.1422	-0.0193	0.1422	-0.0214	0.1422	-0.0257	0.1422	-0.0278	0.1422	-0.0362	0.1422	-0.0404
0.1595	-0.0182	0.1595	-0.0205	0.1595	-0.0251	0.1595	-0.0274	0.1595	-0.0365	0.1595	-0.0411
0.1776	-0.0169	0.1776	-0.0193	0.1776	-0.0243	0.1776	-0.0267	0.1776	-0.0366	0.1776	-0.0416

A3		A4		A6		A7		A11		A13	
X	Y	X	Y	X	Y	X	Y	X	Y	X	Y
0.1964	-0.0154	0.1964	-0.0181	0.1964	-0.0234	0.1964	-0.0260	0.1964	-0.0365	0.1964	-0.0418
0.2160	-0.0139	0.2160	-0.0167	0.2160	-0.0223	0.2160	-0.0251	0.2160	-0.0363	0.2160	-0.0419
0.2362	-0.0122	0.2362	-0.0152	0.2362	-0.0211	0.2362	-0.0241	0.2362	-0.0359	0.2362	-0.0418
0.2570	-0.0106	0.2570	-0.0137	0.2570	-0.0199	0.2570	-0.0230	0.2570	-0.0354	0.2570	-0.0416
0.2784	-0.0089	0.2784	-0.0122	0.2784	-0.0186	0.2784	-0.0218	0.2784	-0.0347	0.2784	-0.0412
0.3003	-0.0074	0.3003	-0.0107	0.3003	-0.0174	0.3003	-0.0207	0.3003	-0.0340	0.3003	-0.0407
0.3227	-0.0058	0.3227	-0.0093	0.3227	-0.0161	0.3227	-0.0195	0.3227	-0.0332	0.3227	-0.0400
0.3455	-0.0044	0.3455	-0.0079	0.3455	-0.0149	0.3455	-0.0184	0.3455	-0.0323	0.3455	-0.0393
0.3686	-0.0032	0.3686	-0.0067	0.3686	-0.0138	0.3686	-0.0173	0.3686	-0.0314	0.3686	-0.0385
0.3921	-0.0020	0.3921	-0.0056	0.3921	-0.0127	0.3921	-0.0162	0.3921	-0.0305	0.3921	-0.0376
0.4158	-0.0011	0.4158	-0.0046	0.4158	-0.0118	0.4158	-0.0153	0.4158	-0.0296	0.4158	-0.0367
0.4397	-0.0001	0.4397	-0.0037	0.4397	-0.0108	0.4397	-0.0144	0.4397	-0.0286	0.4397	-0.0357
0.4638	0.0007	0.4638	-0.0028	0.4638	-0.0099	0.4638	-0.0134	0.4638	-0.0275	0.4638	-0.0346
0.4879	0.0016	0.4879	-0.0019	0.4879	-0.0089	0.4879	-0.0124	0.4879	-0.0264	0.4879	-0.0334
0.5121	0.0023	0.5121	-0.0011	0.5121	-0.0080	0.5121	-0.0115	0.5121	-0.0253	0.5121	-0.0322
0.5362	0.0030	0.5362	-0.0003	0.5362	-0.0071	0.5362	-0.0105	0.5362	-0.0241	0.5362	-0.0309
0.5603	0.0037	0.5603	0.0004	0.5603	-0.0062	0.5603	-0.0096	0.5603	-0.0229	0.5603	-0.0295
0.5842	0.0042	0.5842	0.0010	0.5842	-0.0055	0.5842	-0.0087	0.5842	-0.0217	0.5842	-0.0281
0.6079	0.0048	0.6079	0.0016	0.6079	-0.0047	0.6079	-0.0078	0.6079	-0.0204	0.6079	-0.0267
0.6314	0.0051	0.6314	0.0021	0.6314	-0.0040	0.6314	-0.0071	0.6314	-0.0192	0.6314	-0.0253
0.6545	0.0054	0.6545	0.0025	0.6545	-0.0034	0.6545	-0.0063	0.6545	-0.0180	0.6545	-0.0239
0.6773	0.0056	0.6773	0.0028	0.6773	-0.0028	0.6773	-0.0056	0.6773	-0.0169	0.6773	-0.0225
0.6997	0.0057	0.6997	0.0030	0.6997	-0.0023	0.6997	-0.0050	0.6997	-0.0157	0.6997	-0.0211
0.7216	0.0058	0.7216	0.0033	0.7216	-0.0018	0.7216	-0.0044	0.7216	-0.0146	0.7216	-0.0197
0.7430	0.0057	0.7430	0.0033	0.7430	-0.0015	0.7430	-0.0039	0.7430	-0.0136	0.7430	-0.0184
0.7638	0.0056	0.7638	0.0033	0.7638	-0.0012	0.7638	-0.0035	0.7638	-0.0125	0.7638	-0.0170
0.7840	0.0054	0.7840	0.0033	0.7840	-0.0009	0.7840	-0.0031	0.7840	-0.0115	0.7840	-0.0157
0.8036	0.0051	0.8036	0.0032	0.8036	-0.0008	0.8036	-0.0027	0.8036	-0.0106	0.8036	-0.0145
0.8224	0.0048	0.8224	0.0030	0.8224	-0.0006	0.8224	-0.0024	0.8224	-0.0096	0.8224	-0.0132
0.8405	0.0044	0.8405	0.0028	0.8405	-0.0005	0.8405	-0.0022	0.8405	-0.0088	0.8405	-0.0121
0.8578	0.0040	0.8578	0.0026	0.8578	-0.0004	0.8578	-0.0019	0.8578	-0.0079	0.8578	-0.0109
0.8743	0.0036	0.8743	0.0023	0.8743	-0.0004	0.8743	-0.0018	0.8743	-0.0071	0.8743	-0.0098
0.8898	0.0031	0.8898	0.0019	0.8898	-0.0004	0.8898	-0.0016	0.8898	-0.0064	0.8898	-0.0088
0.9045	0.0027	0.9045	0.0016	0.9045	-0.0005	0.9045	-0.0015	0.9045	-0.0057	0.9045	-0.0078
0.9182	0.0022	0.9182	0.0013	0.9182	-0.0005	0.9182	-0.0014	0.9182	-0.0051	0.9182	-0.0069
0.9310	0.0017	0.9310	0.0009	0.9310	-0.0006	0.9310	-0.0014	0.9310	-0.0045	0.9310	-0.0060
0.9427	0.0013	0.9427	0.0006	0.9427	-0.0007	0.9427	-0.0013	0.9427	-0.0039	0.9427	-0.0052
0.9534	0.0008	0.9534	0.0003	0.9534	-0.0008	0.9534	-0.0013	0.9534	-0.0034	0.9534	-0.0045
0.9631	0.0004	0.9631	0.0000	0.9631	-0.0008	0.9631	-0.0013	0.9631	-0.0030	0.9631	-0.0038
0.9717	0.0001	0.9717	-0.0003	0.9717	-0.0009	0.9717	-0.0013	0.9717	-0.0026	0.9717	-0.0032
0.9791	-0.0003	0.9791	-0.0005	0.9791	-0.0010	0.9791	-0.0013	0.9791	-0.0022	0.9791	-0.0027
0.9855	-0.0006	0.9855	-0.0007	0.9855	-0.0011	0.9855	-0.0013	0.9855	-0.0019	0.9855	-0.0023

A3		A4		A6		A7		A11		A13	
X	Y	X	Y	X	Y	X	Y	X	Y	X	Y
0.9907	-0.0008	0.9907	-0.0009	0.9907	-0.0011	0.9907	-0.0013	0.9907	-0.0017	0.9907	-0.0019
0.9948	-0.0010	0.9948	-0.0011	0.9948	-0.0012	0.9948	-0.0013	0.9948	-0.0015	0.9948	-0.0016
0.9977	-0.0008	0.9977	-0.0008	0.9977	-0.0009	0.9977	-0.0010	0.9977	-0.0012	0.9977	-0.0013
0.9994	-0.0003	0.9994	-0.0003	0.9994	-0.0005	0.9994	-0.0006	0.9994	-0.0009	0.9994	-0.0011
1.0000	-0.0001	1.0000	-0.0002	1.0000	-0.0004	1.0000	-0.0004	1.0000	-0.0008	1.0000	-0.0010

B. XROTOR Geometry Input File

The geometry input file for the optimized geometry has been reported to this paper through the text input below.

XROTOR VERSION: 7.69

```
Arbitrary blade
! Rho                    Vso                    Rmu                    Alt
1.2260                   340.00                 0.17800E-04            0.0000
! Rad                    Vel                    Adv                    Rake
0.22860                  9.1440                 0.12730                0.0000
! XI0                                                                  XIW
0.20031                                                                0.16000
! Naero
15
! Xisection
0.0000
! A0deg                 dCLdA                  CLmax                  CLmin
-3.6197                  6.7350                 1.6140                 -0.34140
! dCLdAstall            dCLstall               Cmconst                Mcrit
0.10000                  0.10000                -0.10000               0.80000
! CDmin                 CLCDmin                dCDdCL^2               dCDdM^2
0.22930E-01              0.50000                0.28700E-02            0.0000
! REref                                                                 REexp
0.10000E+06                                                            -0.40000
! Xisection
0.20000
! A0deg                 dCLdA                  CLmax                  CLmin
-3.6197                  6.7350                 1.6140                 -0.34140
! dCLdAstall            dCLstall               Cmconst                Mcrit
0.10000                  0.10000                -0.10000               0.80000
! CDmin                 CLCDmin                dCDdCL^2               dCDdM^2
0.22930E-01              0.50000                0.28700E-02            0.0000
! REref                                                                 REexp
0.10000E+06                                                            -0.40000
! Xisection
0.72000
! A0deg                 dCLdA                  CLmax                  CLmin
-3.6197                  6.7350                 1.6140                 -0.34140
! dCLdAstall            dCLstall               Cmconst                Mcrit
0.10000                  0.10000                -0.10000               0.80000
! CDmin                 CLCDmin                dCDdCL^2               dCDdM^2
0.22930E-01              0.50000                0.28700E-02            0.0000
! REref                                                                 REexp
0.10000E+06                                                            -0.40000
! Xisection
0.74000
! A0deg                 dCLdA                  CLmax                  CLmin
-3.6462                  6.6759                 1.6000                 -0.33270
! dCLdAstall            dCLstall               Cmconst                Mcrit
0.10000                  0.10000                -0.10000               0.80000
! CDmin                 CLCDmin                dCDdCL^2               dCDdM^2
0.22780E-01              0.50000                0.22900E-02            0.0000
! REref                                                                 REexp
0.10000E+06                                                            -0.40000
! Xisection
0.78000
```

! A0deg	dCLdA	CLmax	CLmin
-3.6462	6.6759	1.6000	-0.33270
! dCLdAstall	dCLstall	Cmconst	Mcrit
0.10000	0.10000	-0.10000	0.80000
! CDmin	CLCDmin	$dCDdCL^2$	$dCDdM^2$
0.22780E-01	0.50000	0.22900E-02	0.0000
! REref			REexp
0.10000E+06			-0.40000
! Xisection			
0.80000			
! A0deg	dCLdA	CLmax	CLmin
-3.7257	6.5990	1.5860	-0.33310
! dCLdAstall	dCLstall	Cmconst	Mcrit
0.10000	0.10000	-0.10000	0.80000
! CDmin	CLCDmin	$dCDdCL^2$	$dCDdM^2$
0.22600E-01	0.50000	0.27400E-02	0.0000
! REref			REexp
0.10000E+06			-0.40000
! Xisection			
0.82000			
! A0deg	dCLdA	CLmax	CLmin
-3.7257	6.5990	1.5860	-0.33310
! dCLdAstall	dCLstall	Cmconst	Mcrit
0.10000	0.10000	-0.10000	0.80000
! CDmin	CLCDmin	$dCDdCL^2$	$dCDdM^2$
0.22600E-01	0.50000	0.27400E-02	0.0000
! REref			REexp
0.10000E+06			-0.40000
! Xisection			
0.84000			
! A0deg	dCLdA	CLmax	CLmin
-3.7787	6.5379	1.5730	-0.33200
! dCLdAstall	dCLstall	Cmconst	Mcrit
0.10000	0.10000	-0.10000	0.80000
! CDmin	CLCDmin	$dCDdCL^2$	$dCDdM^2$
0.22160E-01	0.50000	0.21100E-02	0.0000
! REref			REexp
0.10000E+06			-0.40000
! Xisection			
0.86000			
! A0deg	dCLdA	CLmax	CLmin
-3.8052	6.4730	1.5580	-0.33100
! dCLdAstall	dCLstall	Cmconst	Mcrit
0.10000	0.10000	-0.10000	0.80000
! CDmin	CLCDmin	$dCDdCL^2$	$dCDdM^2$
0.21750E-01	0.50000	0.24840E-02	0.0000
! REref			REexp
0.10000E+06			-0.40000
! Xisection			
0.88000			
! A0deg	dCLdA	CLmax	CLmin
-3.8317	6.4427	1.5510	-0.33300
! dCLdAstall	dCLstall	Cmconst	Mcrit
0.10000	0.10000	-0.10000	0.80000

! CDmin	CLCDmin	$dCDdCL^2$	$dCDdM^2$
0.21400E-01	0.50000	0.24700E-02	0.0000
! REref			REexp
0.10000E+06			-0.40000
! Xisection			
0.90000			
! A0deg	dCLdA	CLmax	CLmin
-3.8582	6.3348	1.5230	-0.34100
! dCLdAstall	dCLstall	Cmconst	Mcrit
0.10000	0.10000	-0.10000	0.80000
! CDmin	CLCDmin	$dCDdCL^2$	$dCDdM^2$
0.20750E-01	0.50000	0.29300E-02	0.0000
! REref			REexp
0.10000E+06			-0.40000
! Xisection			
0.92000			
! A0deg	dCLdA	CLmax	CLmin
-3.8846	6.2573	1.5030	-0.34300
! dCLdAstall	dCLstall	Cmconst	Mcrit
0.10000	0.10000	-0.10000	0.80000
! CDmin	CLCDmin	$dCDdCL^2$	$dCDdM^2$
0.20100E-01	0.50000	0.21970E-02	0.0000
! REref			REexp
0.10000E+06			-0.40000
! Xisection			
0.94000			
! A0deg	dCLdA	CLmax	CLmin
-3.9111	6.1584	1.4780	-0.34600
! dCLdAstall	dCLstall	Cmconst	Mcrit
0.10000	0.10000	-0.10000	0.80000
! CDmin	CLCDmin	$dCDdCL^2$	$dCDdM^2$
0.19510E-01	0.50000	0.22611E-02	0.0000
! REref			REexp
0.10000E+06			-0.40000
! Xisection			
0.96000			
! A0deg	dCLdA	CLmax	CLmin
-3.9341	6.1065	1.4650	-0.35100
! dCLdAstall	dCLstall	Cmconst	Mcrit
0.10000	0.10000	-0.10000	0.80000
! CDmin	CLCDmin	$dCDdCL^2$	$dCDdM^2$
0.19110E-01	0.50000	0.23080E-02	0.0000
! REref			REexp
0.10000E+06			-0.40000
! Xisection			
0.98000			
! A0deg	dCLdA	CLmax	CLmin
-3.9641	6.0433	1.4490	-0.35700
! dCLdAstall	dCLstall	Cmconst	Mcrit
0.10000	0.10000	-0.10000	0.80000
! CDmin	CLCDmin	$dCDdCL^2$	$dCDdM^2$
0.18830E-01	0.50000	0.24820E-02	0.0000
! REref			REexp
0.10000E+06			-0.40000

! LFree		LDuct	LWind
! T		F	F
! II			Nblds
41			2
! r/R	c/R	$\beta(deg)$	Ubody
0.20	0.193122679888889	49.8651045114910	0.0000
0.22	0.195811712111111	47.4433764936053	0.0000
0.24	0.198500744444444	45.3301551664401	0.0000
0.26	0.200824610222222	43.4748069181257	0.0000
0.28	0.202393945444444	41.8361096610741	0.0000
0.30	0.203062202888889	40.3804755927518	0.0000
0.32	0.202916391000000	39.0804518925013	0.0000
0.34	0.202360777555556	37.9134995842116	0.0000
0.36	0.201399900777778	36.8610168549042	0.0000
0.38	0.200006827111111	35.9075647160367	0.0000
0.40	0.198058903222222	35.0402550723741	0.0000
0.42	0.195883152888889	34.2482670617697	0.0000
0.44	0.193476029777778	33.5224639094709	0.0000
0.46	0.190820545888889	32.8550883147038	0.0000
0.48	0.187907251222222	32.2395192018731	0.0000
0.50	0.184929086666667	31.6700765208144	0.0000
0.52	0.181889727000000	31.1418637947368	0.0000
0.54	0.178789081888889	30.6506404449851	0.0000
0.56	0.175580677555556	30.1927177130073	0.0000
0.58	0.172316327555556	29.7648733737447	0.0000
0.60	0.168991960333333	29.3642814886475	0.0000
0.62	0.165588089333333	28.9884542566438	0.0000
0.64	0.162168486333333	28.6351936459080	0.0000
0.66	0.158720220222222	28.3025509724691	0.0000
0.68	0.155237022333333	27.9887929670903	0.0000
0.70	0.151702183666667	27.6923731647645	0.0000
0.72	0.147951833444444	27.4119076807816	0.0000
0.74	0.144126087666667	26.5157499986203	0.0000
0.76	0.140252605444444	26.0963608244015	0.0000
0.78	0.136320347444444	25.5375982251760	0.0000
0.80	0.132329633333333	24.5409424506517	0.0000
0.82	0.128318285333333	23.5269448189502	0.0000
0.84	0.124298202333333	22.4859304790347	0.0000
0.86	0.120265724888889	21.0135888592329	0.0000
0.88	0.116134799000000	19.9454615039206	0.0000
0.90	0.111892125555556	18.8546056060364	0.0000
0.92	0.107520531555556	17.8980566525157	0.0000
0.94	0.102948993000000	15.7832304650113	0.0000
0.96	0.097893002444445	12.3116297479523	0.0000
0.98	0.086705406888889	9.5216134721156	0.0000
0.99	0.064516129000000	6.3964604937789	0.0000
! URDuct			
1.0000			